Resonance Raman Investigation of Fe−N−O Structure of Nitrosylheme in Myoglobin and Its Mutants

Takeshi Tomita,[†] Shun Hirota,[‡] Takashi Ogura,[||] John S. Olson,[⊥] and Teizo Kitagawa*

The Graduate University for Advanced Studies and Institute for Molecular Science, Okazaki National Research Institutes, Myodaiji, Okazaki, 444-8585 Japan, and Department of Biochemistry and Cell Biology, Rice University, Houston, Texas 77005-1892

Received: March 30, 1999; In Final Form: May 21, 1999

Resonance Raman spectra have been observed for NO adducts of wild-type (WT) sperm whale myoglobin (MbNO) and its H64G, H64L, L29W, V68W, and V68T mutants at neutral and acidic pH. Raman excitation in resonance with the Soret band enabled us to detect the Fe−NO stretching (ν_{Fe-NO}), N−O stretching (ν_{NO}), and Fe−N−O bending (δ_{FeNO}) bands. The ν_{Fe-NO}, δ_{FeNO}, and ν_{NO} bands of WT MbNO at neutral pH were observed at 560, 452, and 1613 cm^{-1}, respectively, and substitution of the distal His64 to Gly or Leu caused an upshift of ν_{NO} to 1631−1635 cm^{-1} but no change in ν_{Fe-NO}. This change in ν_{NO} is considered to be due to the removal of hydrogen bonding between His64 and bound NO. Conversely, substitution of Leu29 with tryptophan (L29W) altered ν_{Fe-NO} but caused no change in ν_{NO} at neutral pH. This feature resembles that of MbO_2 but distinctly differs from that of MbCO, for which the Fe−CO and C−O stretching frequencies have an inverse linear correlation. The change in ν_{Fe-NO} for L29W−MbNO is probably caused by tilting of the Fe−N bond from the heme normal on account of steric hindrance from the large indole ring but would not be due to changes in the Fe−N−O bond angle. When pH is lowered to 4, MbNO adopts the five-coordinate structure due to cleavage of the Fe−His bond. Accordingly, the heme maker bands such as ν_3 and ν_{10}, shifted from 1500 and 1636 cm^{-1} at pH 7.4 to 1509 and 1646 cm^{-1} at pH 4 which are in agreement with those of a five-coordinate Fe−protoporphyrin−NO complex in detergent micelles at neutral pH. The ν_{Fe-NO} and ν_{NO} bands of acidic MbNO were observed at 520 and 1668 cm^{-1} and exhibited no shift when the distal His was replaced by Gly or Leu. The latter observation supports previous X-ray crystallographic, infrared, and resonance Raman spectroscopic measurements which show that the distal histidine becomes protonated at pH 4 and swings out into the solvent away from the bound ligand.

Introduction

Interactions of nitric oxide (NO) with a heme in proteins have increasingly attracted chemists' attention since the discoveries of its generation from L-arginine by a heme enzyme named nitric oxide synthase (NOS)[1−3] and of its binding to a heme of a receptor protein named soluble guanylyl cyclase (sGC).[4] Both NOS and sGC contain an Fe−protoporphyrin IX complex similar to myoglobin (Mb). For NOS the presence of some feed back regulation by binding of generated NO to the heme has been noted from resonance Raman studies.[5] For sGC the up-regulation by NO-binding to heme is well-known,[6] and recently we pointed out a possibility of down-regulation by the enzymatic product, in which the binding of cyclic GMP (cGMP) to the NO adduct (sGC−NO) caused a frequency shift of N−O stretching mode (ν_{NO}) of bound NO.[7] These are all in consequence of the interactions of NO with a heme and surrounding amino acid residues, and accordingly, physicochemical characterization of interactions of a nitrosylheme with proteins is desirable.

Mb is one of the best characterized proteins, and the effects of individual amino acid residues on ligand binding have been studied in detail using a method of site directed mutagenesis.[8,9] NO binds to the ferrous heme with much higher affinity than CO or O_2 does.[10,11] NO can also make an adduct with ferric Mb, but its affinity ($K_d \sim 1 \times 10^{-4}$ [M^{-1}]) is much lower than that of ferrous hemes ($K_d \sim 1 \times 10^{-14}$ [M^{-1}]). Moreover, ferric Mb−NO[Mb(III)−NO] undergoes reductive nitrosylation, in which the reductive dissociation of NO from a ferric heme is accompanied by association of another NO, generating ferrous nitrosylmyoglobin [MbNO].[12]

One of the important factors which control the reactivity of bound NO in heme proteins seems to be the trans Fe−ligand bond. Hemoglobin (Hb) with histidine (His)-coordinated hemes has two distinct quaternary structures (T and R) with different oxygen affinity[13] and different Fe−His bond strengths; the Fe−His bond is weaker in the T state than that in the R state and in the α than β subunit within the T state owing to the strain by globin.[14a,b] The NO-bound Hb contains the six-coordinated hemes in the R state but has the five- (α) and six-coordinated (β) hemes in the T state.[15,16] The Fe−His bond of sGC is weaker than those of other heme proteins judging from its Fe−His stretching (ν_{Fe-His}) frequency (203 cm^{-1})[7,17] and is quickly cleaved upon binding of NO at neutral pH.[18] The ν_{Fe-His} frequency of ferrous FixL is also low (212 cm^{-1}),[19a] and its NO adduct is reported to be a mixture of six- and five-coordinate

* To whom correspondence should be addressed.
[†] Present address: Institute for Chemical Reaction Science, Tohoku University, Katahira, Aoba-ku, Sendai, 980-8577.
[‡] Present address: Department of Chemistry, Graduate School of Science, Nagoya University, Chikusa-ku, Nagoya, 464-8602 Japan.
[||] Present address: Tokyo University, Komaba, Meguro-ku, Tokyo, 153-8902.
[⊥] Department of Biochemistry and Cell Biology.

10.1021/jp991106n CCC: $18.00
Published on Web 08/03/1999

complexes.[19b,20] The strength of Fe−His bond of deoxyMb is medium (ν_{Fe-His} = 220 cm^{-1})[21a] and the six-coordinated nitrosylheme is stable for Mb(II)−NO at neutral pH, although the Fe−His bond is cleaved at acidic pH.[22] The Fe−His bond of horseradish peroxidase (HRP) is the strongest among His-coordinated heme proteins (ν_{Fe-His} =244 cm^{-1}),[21b] and its NO adduct adopts the six-coordinated structure even at acidic pH.[23,24]

Distal effects generated by amino acid residues near the coordinated NO are also important. Hydrogen bonding between distal His and the bound NO plays an essential role.[9] The distal His becomes protonated at pH 4.3 and swings out into the solvent away from the bound ligand.[24−26] It is noted that there is some communication linkage between the distal and proximal sides through hydrogen bond networks as demonstrated for HRP.[27] Therefore, a structural change in the distal side upon NO binding can potentially be communicated to the proximal side through a polypeptide backbone. However, recent studies with site directed mutagenesis of Mb have demonstrated that replacement of selected amino acid residues (positions 29, 64, and 68) in the distal side greatly changes the affinity of ligand without changing the Fe−His bond strength.[9,28] Accordingly, in this study, we have examined the resonance Raman (RR) spectra of NO adducts of these Mb mutants in focus on the ν_{Fe-NO} and ν_{NO} bands to elucidate the RR spectra of sGC−NO.

Materials and Methods

Materials. The stock solution of horse heart (hh) Mb was prepared by dissolving lyophilized Mb (type III, Sigma) into 50 mM sodium phosphate buffer pH 7.4 containing potassium ferricyanide, and the ferricyanide was removed by gel filtration through Sephadex G-25 equilibrated previously with sodium phosphate buffer. The experimental procedures of site-directed mutagenesis of sperm whale (sw) Mb have been described separately.[29] Purified recombinant Mbs were stored at −80 °C as CO-bound form (MbCO) and treated in the same way as that for the native hh Mb just before the Raman measurements. The purity of stable isotopes of NO [$^{15}N^{16}O$ (Shoko Tsusho) and $^{15}N^{18}O$ (ICON)] was 99 at. %. Hemin chloride (bovine, Sigma), bovine serum albumin (BSA; =97% essentially fatty acid free, Sigma), cholic acid (biochemical grade, Nakalai Tesque), and other reagents (Wako Pure Chemicals) were used as purchased unless otherwise stated.

Preparation of Nitrosylmyoglobin and NitrosylFe−porphyrin. A stock solution of Fe−protoporphyrin IX [Fe(PPIX)] (10 mM) was prepared by dissolving hemin chloride into 0.1 M NaOH and was used within 6 h. For the measurements of Raman spectra, the stock solution was diluted to 80 μM by 50 mM triethanolamine (TEA) aqueous solution, pH 7.4 containing 0.5% BSA or 0.5% sodium cholate, and pH was readjusted to 7.4. For Mb, the stock solution was diluted to 50 μM by 50 mM phosphate buffer, pH 7. The diluted solution (100 μL) was put into an airtight spinning cell and deoxygenated by repeated evacuation and flushing with pure nitrogen gas. After the addition of sodium dithionite solution to the cell with a final concentration of 2−5 mM, NO gas, which had been vigorously shaken with 1 M NaOH solution in advance, was incorporated into the Raman cell through a rubber septum with an airtight syringe. Degassed acetic acid (0.6 μL) was added with another airtight syringe to obtain acidic solutions.

Measurements of Resonance Raman Spectra. Raman scattering was excited with the 406.7 nm line of a Kr^+ ion laser (Spectra Physics, Model 2016) or the 422.6 nm line of an intracavity frequency-doubled Cr:$LiSrAlF_6$ laser pumped by a diode laser (Hitachi Metals, model ICD-430) and was detected by a cooled intensified photodiode array (PAR, 1421HQ) or a charge coupled device (CCD) (Astromed, CCD 3200) attached to a single polychromator (Ritsu Oyo Kogaku, DG-1000). The Raman excitation beam was introduced from the bottom of a Raman cell, and the scattered radiation along 90° from the incident radiation was collected. The slit width was 200 μm and temperature was kept at 20 °C for all the measurements. The Raman shifts were calibrated with toluene and carbon tetrachloride, which were precalibrated with indene. UV−vis absorption spectra were measured with a Hitachi U-3210 spectrophotometer.

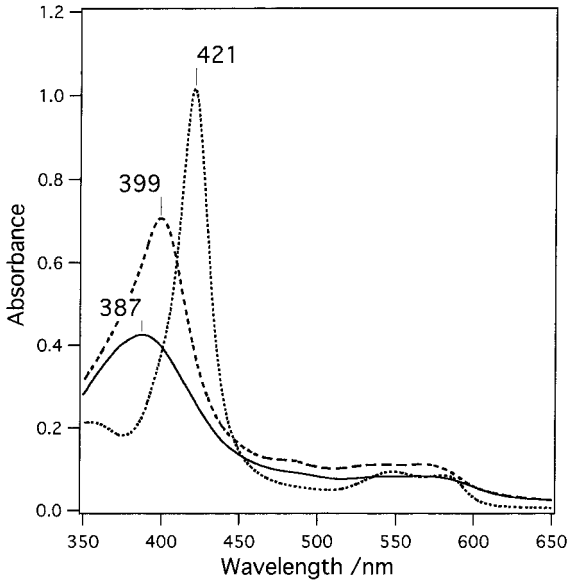

Figure 1. Absorption spectra of horse heart MbNO and Fe^{II}(PPIX)−NO. Dotted line and bold line represent absorption spectra of Mb−NO (8 μM) at pH 7.4 and pH 4, respectively. Dashed line represents that of Fe^{II}(PPIX)−NO (8 μM) in 50 mM TEA, pH 7.4, 0.5% sodium cholate. Path length was 10 mm.

Results

The UV−vis absorption spectra of Fe^{II}(PPIX)-NO at pH 7.4 and native hh MbNO at pH 7.4 and pH 4 are shown in Figure 1. The Soret peak of the five-coordinated Fe^{II}(PPIX)−NO complex (399 nm) did not shift between pH 7.4 and 3.3. In contrast, acidification of MbNO caused a shift of the Soret peak from 421 nm at pH 7.4 to 387 nm at pH 4 and intensity reduction, in agreement with the reported results.[22] It was noted previously that a cavity mutant of Mb, H93G, formed the five-coordinated heme−NO adduct at neutral pH and its Soret band was observed at 400 nm with reduced intensity[30] similar to Fe^{II}(PPIX)−NO in an aqueous solution.

Figure 2 shows the RR spectra of hh MbNO at pH 7.4 in the (a) 300−650 and (b) 1450−1700 cm^{-1} regions, where spectra A and B display the results obtained with $^{14}N^{16}O$ and $^{15}N^{16}O$, respectively, and spectra C and D are differences of $^{14}N^{16}O$ minus $^{15}N^{16}O$ and $^{15}N^{16}O$ minus $^{15}N^{18}O$, respectively. The ν_4 (not shown), ν_3, and ν_{10} bands appear at 1375, 1500, and 1635 cm^{-1}, respectively, in (b) and they serve as markers for the six-coordinate nitrosylheme complex.[16b] The isotope-difference spectra reveal the presence of NO-isotope sensitive bands at 1613 (Mb−$^{14}N^{16}O$), 1586 (Mb−$^{15}N^{16}O$), and 1545 cm^{-1} (Mb−$^{15}N^{18}O$), which are assigned to ν_{NO}. Although the ν_{NO} mode of MbNO was previously reported at different frequencies from Raman[31] and IR[32] measurements (1624 and 1612 cm^{-1},

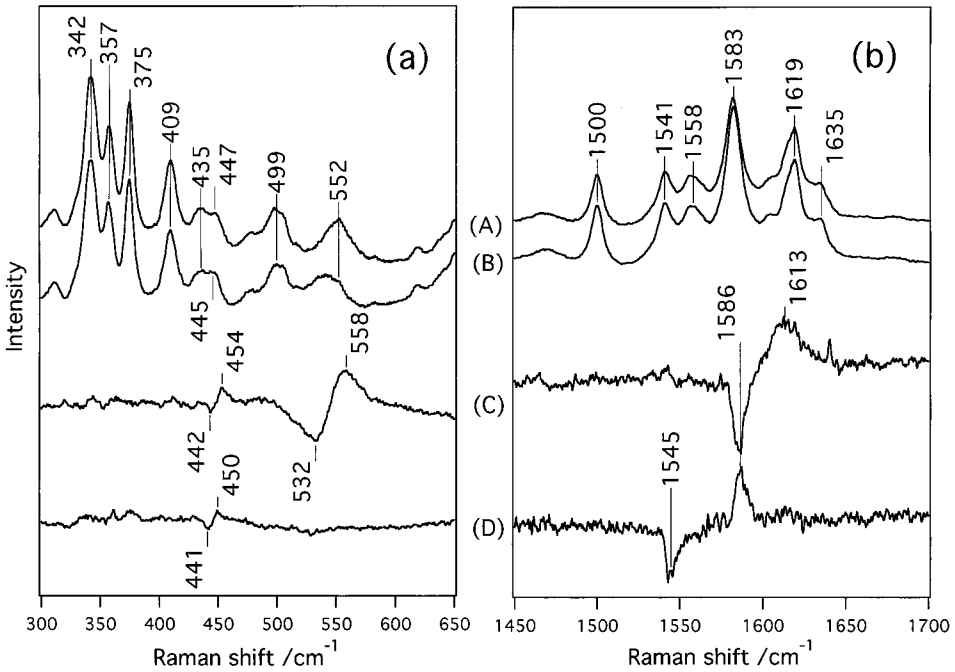

Figure 2. Raman spectra in the 300−650 (a) and 1450−1700 cm^{-1} regions (b) of horse heart Mb−NO (50 μM) in 50 mM sodium phosphate, pH 7.4. (A) Mb−$^{14}N^{16}O$, (B) Mb−$^{15}N^{16}O$, (C) difference spectrum [= {(A) − (B)} × 2 for (a) and {(A) − (B)} × 6 for (b)], and (D) difference spectrum, Mb−$^{15}N^{16}O$ − Mb−$^{15}N^{18}O$. Experimental conditions: temperature, 20 °C; excitation, 406.7 nm and 5 mW at sample; accumulation time, 5 min.

respectively), the present results with $^{14}N^{16}O$ support the IR value,[32] but those with $^{15}N^{16}O$ agree with the Raman value (1587 cm^{-1}).[31] The ^{15}N-isotopic frequency shift of ν_{NO} in this work (27 cm^{-1}) is more reasonable than the reported Raman value (37 cm^{-1}),[31] which is beyond the maximum frequency shift expected for a diatomic NO molecule (29 cm^{-1}).

In the lower frequency region (a), the isotope-sensitive bands are observed at 558 and 454 cm^{-1} for Mb−$^{14}N^{16}O$, at 532 and 442 cm^{-1} for Mb−$^{15}N^{16}O$, and at 441 cm^{-1} for Mb−$^{15}N^{18}O$, and a similar difference spectrum of $^{14}N^{16}O$−$^{15}N^{18}O$ (not shown) showed positive peaks at 558 and 453 cm^{-1} and negative peaks at 531 and 442 cm^{-1}. The results are similar to those of $P450_{cam}NO$,[33,34] for which the high- and low-frequency bands are assigned to the Fe−NO stretching (ν_{Fe-NO})[31b] and Fe−N−O bending (δ_{FeNO}) modes,[33a] respectively. Accordingly, the 558 and 454 cm^{-1} bands for Mb−$^{14}N^{16}O$ are assigned to the ν_{Fe-NO}, and δ_{FeNO}, respectively. Although the latter was too weak to determine its band position in the absolute spectra, its presence around 450 cm^{-1} is undoubted. The absence of the ν_{Fe-NO} difference peak in the difference spectrum between $^{15}N^{16}O$ and $^{15}N^{18}O$ [Figure 2a, trace D] despite of the presence of the δ_{FeNO} difference peak is due to a broad feature of the band compared with the size of frequency shift. The small frequency shift means that the ν_{Fe-NO} frequency is sensitive to the mass of N but insensitive to the mass of O, suggesting a significantly bent geometry of Fe^{II}−N−O.

Figure 3 shows the RR spectra of MbNO in the 400−650 cm^{-1} region for the $^{14}N^{16}O$-adducts of (A) WT−, (B) Gly64−, (C) Leu64−, (D) Trp29−, (E) Thr68−, and (F) Trp68−Mbs at (a) pH 7.4 and (b) their $^{14}N^{16}O$−$^{15}N^{16}O$ isotope-difference spectra. The ν_{Fe-NO} band of recombinant WT sw (b) MbNO is observed at 560/532 cm^{-1} for $^{14}N^{16}O/^{15}N^{16}O$. The peak positions of ν_{Fe-NO} bands of (B) Gly64− and (C) Leu64−MbNO are almost the same as that of WT MbNO but those of (D) Trp29−, (E) Thr68−, and (F) Trp68−MbNO are appreciably different. The trends of change in band positions are seen in the (a) raw spectra but are obscured on account of overlapping with a porphyrin band around 550 cm^{-1}. There are another difference features around 450 cm^{-1} in individual difference spectra, although weak. They are caused by the presence of δ_{FeNO} band.

Figure 4 shows the raw RR spectra in the 1450−1700 cm^{-1} region for the $^{14}N^{16}O$-adducts of (A) WT−, (B) Gly64−, (C) Leu64−, (D) Trp29−, (E) Thr68−, and (F) Trp68−Mbs at (a) pH 7.4 and their (b) $^{14}N^{16}O$−$^{15}N^{16}O$-isotope difference spectra. The raw spectra of these mutants are apparently alike, but their differences are clearer in the isotope difference spectra. The ν_{NO} band of recombinant (A) WT sw MbNO was observed at 1613/1586 cm^{-1} for $^{14}N^{16}O/^{15}N^{16}O$, at the same frequencies as those of native hh MbNO (Figure 2b). In contrast with the similarity in the patterns of the ν_{Fe-NO} difference spectra for various mutants, their patterns of ν_{NO} difference spectra are different and seem to depend on a position of mutation; (B) Gly64− and (C) Leu64−MbNO yield two negative and a single positive peaks, (D) Trp29− gives one negative and two positive peaks, and (E) Thr68−, and (F) Trp68−MbNO give two positive and two negative peaks. Since the porphyrin ν_3 band at 1500 cm^{-1} is completely canceled in all of these difference spectra, it is unlikely that the porphyrin bands remain unsubtracted. Presumably the intrinsic ν_{NO} frequency of mutant MbNOs is primarily determined by the position of mutation, but this vibration is weakly coupled with a porphyrin vibration. When the intrinsic ν_{NO} frequency is altered by isotope substitution or mutation and happens to come close to a frequency of the totally symmetric porphyrin modes, the vibrational coupling becomes noticeable. If the coupling counterpart has strong Raman intensity as those at 1619 (vinyl) and 1583 (ν_2) cm^{-1}, the coupling might influence its intensity slightly with a small change of its frequency. Then, additional peak beside ν_{NO} would appear in the NO-isotope difference spectrum at a frequency close to a peak in the raw spectrum. This would be the case of Figure 4b. To confirm such an idea, we examined one mutant in detail.

Figure 5 shows the RR spectra of (A) Leu64−$Mb^{14}N^{16}O$ and (B) Leu64−$Mb^{15}N^{16}O$ and the differences, (C) $^{14}N^{16}O$−$^{15}N^{16}O$

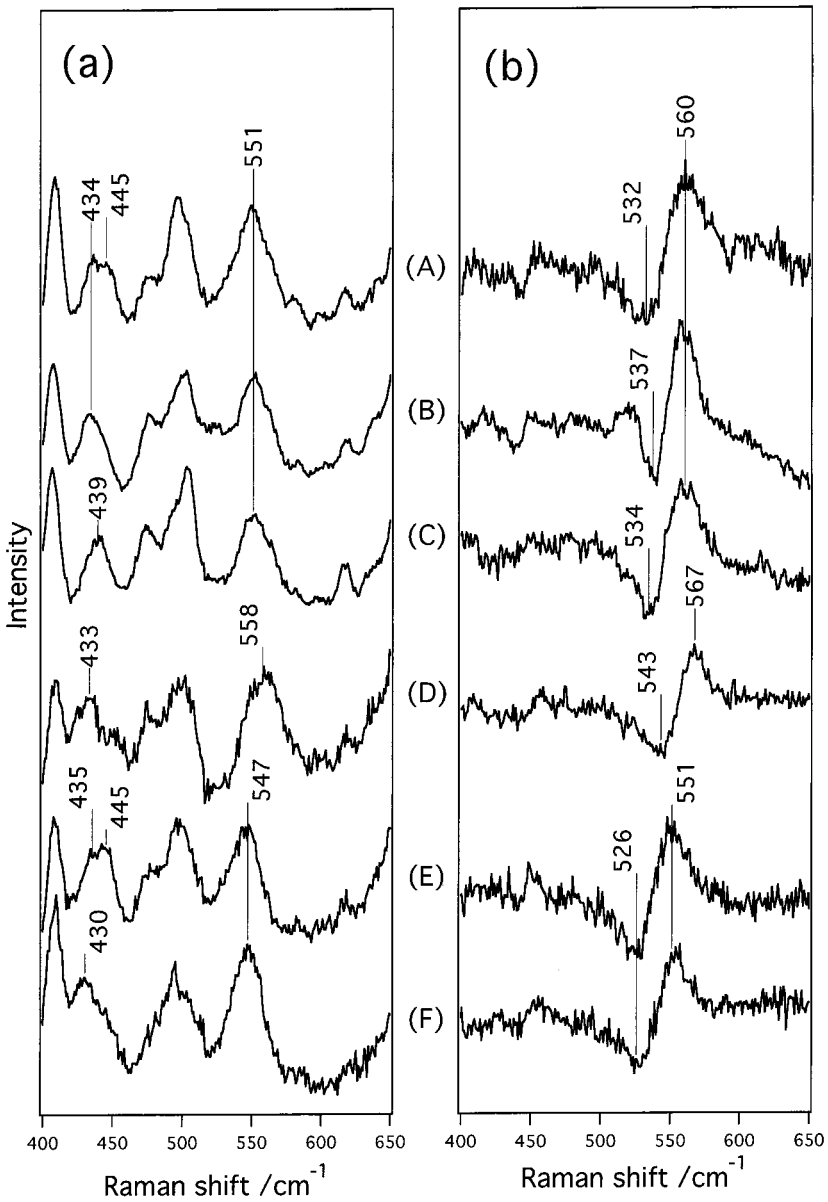

Figure 3. Raman spectra in the 400−650 cm^{-1} region (a) of recombinant sperm whale Mb(II)-NOs (50 μM) in 50 mM sodium phosphate, pH 7.4. and their Mb−$^{14}N^{16}O$ minus Mb−$^{15}N^{16}O$ difference spectra. (A) wild type, (B) Gly64−, (C) Leu64−, (D) Trp29−, (E) Thr68− and (F) Trp68− MbNOs. The difference spectra are expanded in the ordinate by a factor of 4. Experimental conditions are the same as those for Figure 2.

and (D) $^{15}N^{16}O-^{15}N^{18}O$. Note that the spectral pattern of negative side of trace C differs from that of positive side of trace D, despite the fact that both should reflect the spectrum of Mb$^{15}N^{16}O$ molecule. If a Raman inactive mode were coupled with the N−O stretching mode and borrowed Raman intensity from the N−O stretch, or if there were two conformations with different ν_{NO} frequencies, the negative spectrum of trace C should agree with the positive spectrum of trace D. The disagreement suggests a different mechanism.

If the isotopic frequency shifts in Leu64−MbNO are similar to those of WT−MbNO (Figure 2, $^{14}N^{16}O-^{15}N^{16}O = 27$ cm^{-1} and $^{15}N^{16}O-^{15}N^{18}O = 41$ cm^{-1}), we may be allowed to assume the unperturbed ν_{NO} frequencies of Leu64−MbNO at 1635, 1610, and 1570 cm^{-1} for $^{14}N^{16}O$, $^{15}N^{16}O$, and $^{15}N^{18}O$, respectively. In this case the isotopic frequency shifts of $^{14}N^{16}O-^{15}N^{16}O = 25$ cm^{-1} and $^{15}N^{16}O-^{15}N^{18}O = 40$ cm^{-1} are within the maximum frequency shift expected for a diatomic NO molecule (29 and 44 cm^{-1}, respectively). When the bent NO group interacts with vinyl side chains and the outer carbon atoms of porphyrin macrocycle, the vinyl stretching at 1617 cm^{-1} and $C_\beta-C_\beta$ stretching (ν_2) at 1582 cm^{-1} would be slightly perturbed due to vibrational mixing. This would be emphasized in the difference spectrum, because the nonperturbed contributions (the other vinyl group, for example) would be canceled in the difference calculations.

The extent of vibrational mixing of ν_{NO} with the vinyl mode would be larger as the ν_{NO} frequency comes closer to the vinyl mode at 1617 cm^{-1}, that is, the order of $^{15}N^{16}O$ > $^{14}N^{16}O$ > $^{15}N^{18}O$. For the stronger mixing, the larger intensity sharing and larger shifts from the intrinsic frequency are expected. Accordingly, the negative peak at 1621 cm^{-1} in spectra C and E and the positive peak around 1620 cm^{-1} in spectrum D are attributed to the vinyl mode interacting with $^{15}N^{16}O$. The frequency is slightly higher (4 cm^{-1}) than the intrinsic frequency and simultaneously the observed ν_{NO} frequency for $^{15}N^{16}O$ is shifted to a lower frequency by 3 cm^{-1}. Because of unknown reasons, the vinyl intensity of Mb$^{15}N^{18}O$ is stronger than those of other species and as a result the positive peak around 1621 cm^{-1} in trace D is weak and the negative peak in spectrum E is intense.

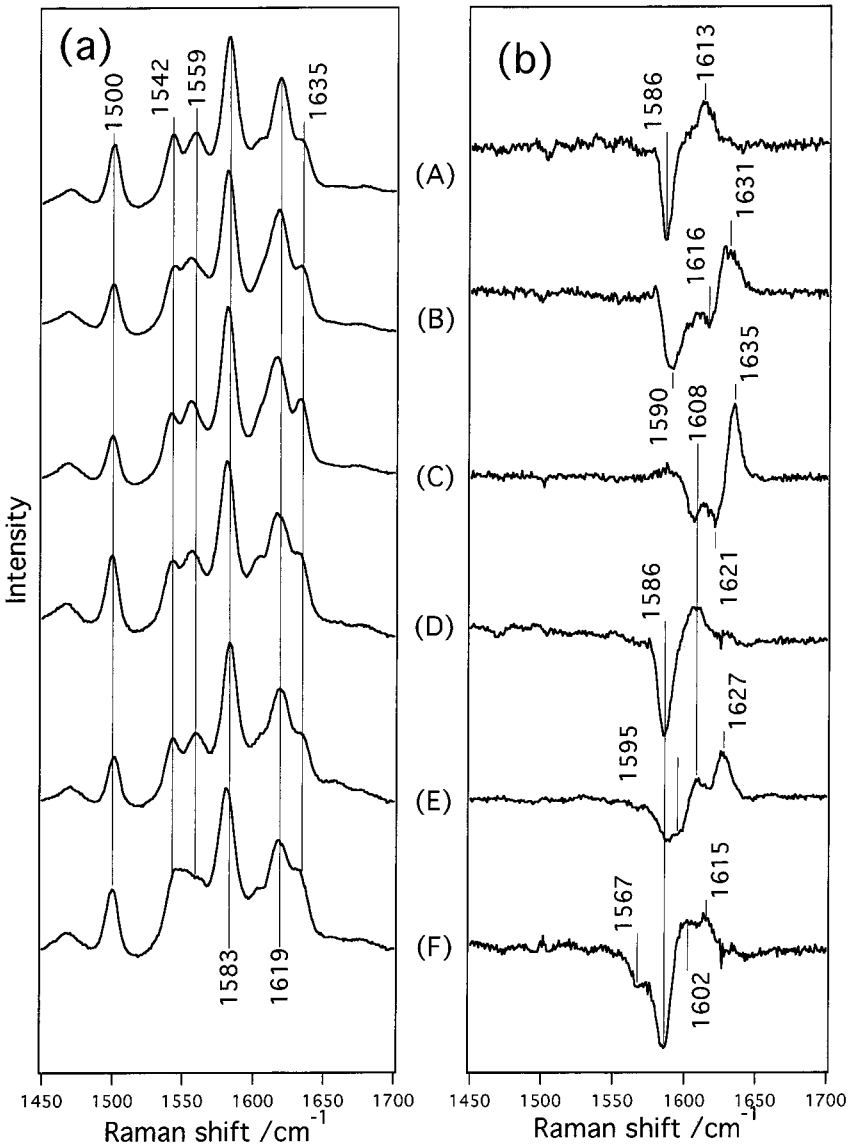

Figure 4. Raman spectra in the 1450−1000 cm^{-1} regions (a) of recombinant sperm whale Mb(II)-NOs (50 μM) in 50 mM sodium phosphate, pH 7.4 and their Mb−$^{14}N^{16}O$ minus Mb−$^{15}N^{16}O$ difference spectra. (A) Wild type, (B) Gly64−, (C) Leu64−, (D) Trp29−, (E) Thr68−, and (F) Trp68−MbNOs. The difference spectra are expanded in the ordinate by a factor of 4. Experimental conditions are the same as those for Figure 2.

Similarly, if the ν_2 mode at 1582 cm^{-1} is mixed with the ν_{NO} mode, the mixing would be largest for $^{15}N^{18}O$ due to proximity of its frequency. In fact, the ν_2 mode is shifted to higher frequency by 4 cm^{-1} and ν_{NO} mode is shifted to a lower frequency by 4 cm^{-1} in spectrum E than those of the intrinsic frequencies. This mixing could be neglected for $^{15}N^{16}O$ and $^{14}N^{16}O$ owing to large separation of frequencies. Thus, the appearance of two negative peaks at 1566 and 1586 cm^{-1} in spectrum E is reasonably interpreted in terms of the interactions between bound NO and porphyrin macrocycle which cause small vibrational mixing.

Figure 6 shows the RR spectra of hh native MbNO at pH 4 in the (a) 300−650 and (b) 1450−1750 cm^{-1} regions for the (A) $^{14}N^{16}O$− and (B) $^{15}N^{16}O$ derivatives and their differences, (C) $^{14}N^{16}O-^{15}N^{16}O$ and (D) $^{15}N^{16}O - {}^{15}N^{18}O$. As shown in part b, the ν_4 (not shown), ν_3, and ν_{10} bands appear at 1375, 1508, and 1645 cm^{-1}, respectively, at pH 4. These frequencies are characteristic of a five-coordinate nitrosylheme.[16b]

The isotope difference spectra C and D demonstrate the presence of isotope sensitive bands at 1668, 1639, and 1595 cm^{-1} for the $^{14}N^{16}O$, $^{15}N^{16}O$, and $^{15}N^{18}O$ derivatives, respectively, which are assigned to ν_{NO}. Therefore, the ν_{NO} frequency is higher for the five-coordinate than six-coordinate structures by 50−55 cm^{-1} (see Figure 2b). In the lower frequency region (part a) the isotope sensitive bands were observed at 524, 511, and 508 cm^{-1} (not shown) for $^{14}N^{16}O$, $^{15}N^{16}O$, and $^{15}N^{18}O$ derivatives, respectively, although in trace D the peak/trough positions are more separated than real band positions because of close proximity of the Fe−$^{15}N^{16}O$ and Fe−$^{15}N^{18}O$ stretching frequencies. These bands are assigned to ν_{Fe-NO}. Their frequencies are lower by 21−34 cm^{-1} than those in the case of the six-coordinate structures (Figure 2a), and the isotopic frequency shifts are much smaller. Here the difference spectrum of $^{15}N^{16}O-^{15}N^{18}O$ gives rise to a differential pattern for ν_{Fe-NO}, mode (a, trace D), although the corresponding peak was not identified for the six-coordinate species (Figure 2a). This is owed to narrow width of the band for the five-coordinate species as will be discussed later. Recently, Babcock and co-workers[35] observed the Fe−N−O bending Raman band of five-coordinated heme−NO complex for the first time; recombinant sGC−NO gave a peak/trough at 402/389 cm^{-1} in the isotope difference spectrum for the $^{14}N^{16}O/^{15}N^{18}O$-adducts. In Figure 6a, trace C, a similar difference pattern is recognizable around 400 cm^{-1}, but we could not determine its peak positions due to weakness.

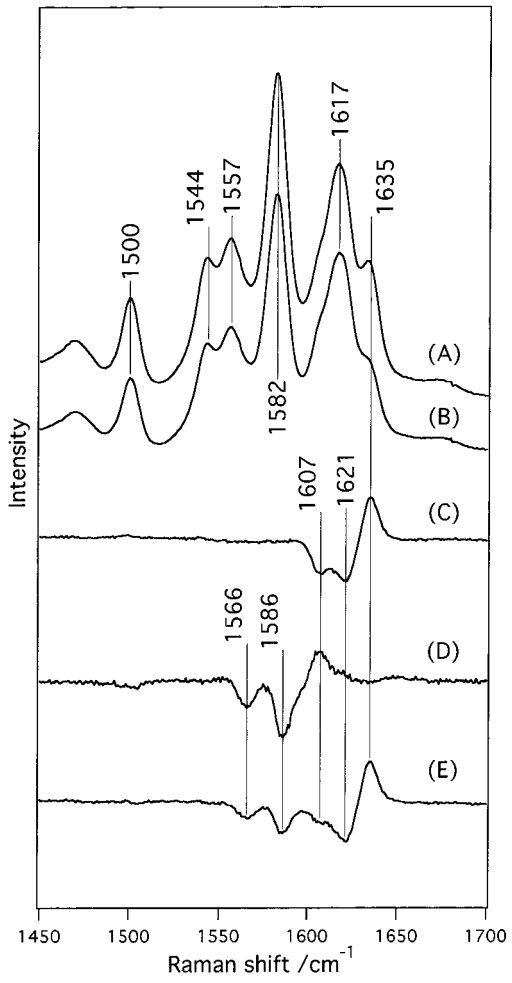

Figure 5. Raman spectra in the 1450−1700 cm^{-1} region of horse heart MbNO (50 μM) in 50 mM sodium phosphate, pH 7.4, and their isotope difference spectra. (A) Mb^{14}N^{16}O, (B) Mb^{15}N^{16}O, (C) difference spectrum, Mb^{14}N^{16}O − Mb^{15}N^{16}O, (D) difference spectrum, Mb^{15}N^{16}O − Mb^{15}N^{18}O, and (E) difference spectrum, Mb^{14}N^{16}O − Mb^{15}N^{18}O. The ordinate scales of different spectra are expanded by a factor of 2 compared with those of (A) and (B). Other conditions are the same as those for Figure 2.

Figure 7 shows the RR spectra of Leu64−MbNO at pH 4 in the (a) 300−800 and (b) 1300−1800 cm^{-1} regions for the (A) ^{14}N^{16}O− and (B) ^{15}N^{16}O derivatives and their difference, (C) ^{14}N^{16}O−^{15}N^{16}O. The ν_{NO} and ν_{Fe-NO} bands for ^{14}N^{16}O/^{15}N^{16}O are seen at 1668/1636 and 523/510 cm^{-1}, respectively, similar to the case of hh native MbNO. It is noted that the NO-isotope difference spectra for WT−, Gly64−, and Trp64−MbNO at pH 4 (not shown) were all quite similar to that of hh native MbNO at pH 4 for both of ν_{NO} and ν_{Fe-NO} in contrast with the results at neutral pH.

To reveal the effects of protein environments on the nitrosylheme of MbNO, the RR spectra of Fe^{II}(PPIX)−NO in aqueous solutions were examined. Fe^{II}(PPIX)−NO immediately aggregated in neutral buffer, but addition of BSA or detergents enabled us to observe the ν_{NO} and ν_{Fe-NO} RR bands in a monomer state. The Raman spectra of Fe^{II}(PPIX)−NO in 50 mM TEA, pH 7.4, with 0.5% sodium cholate are shown in Figure 8. They are quite similar to that of MbNO at pH 4 and it did not show a pH dependent change between pH 7.4 and 3.3. Therefore, the pH dependent RR spectral change of MbNO is not caused by a simple protonation of nearby residues.

The Fe^{II}(PPIX)−NO gave isotope sensitive bands at 1671 and 1641 cm^{-1} in the high-frequency region (Figure 8b) for the ^{14}N^{16}O and ^{15}N^{16}O derivatives, respectively, which were assigned to ν_{NO}. The other isotope-sensitive bands were identified at 527 and 516 cm^{-1} for the ^{14}N^{16}O and ^{15}N^{16}O derivatives (Figure 8a), respectively, which were assigned to ν_{Fe-NO}. The spectral patterns and the NO-associated frequencies of Fe^{II}(PPIX)NO in the presence of BSA were similar to those of cholate-solubilyzed one, but the spectra were of lower quality. It is likely that an Fe^{II}(PPIX)−NO molecule is trapped in a hydrophobic pocket of BSA molecule without forming a covalent bond. In the case of cholate, good spectra were not obtained unless the concentration of cholate was raised to that higher than its critical micelle concentration. It means that Fe^{II}(PPIX)−NO molecules are incorporated into micelles of cholate without forming a covalent bond with cholate. Accordingly, these Fe^{II}(PPIX)−NO molecules are considered to adopt the five coordinate structure with no ligand trans to NO. It is quite reasonable that their ν_{NO} and ν_{Fe-NO} frequencies are close to those of MbNO at pH 4 (Figure 5) rather those at pH 7 (Figure 2). We were unable to prepare a six-coordinate Fe^{II}(PPIX)-(L)NO complex in either aqueous or organic solvents. A summary of the frequencies of all the NO-associated bands and their isotopic shifts in the myoglobin and model complexes are given in Table 1.

Figure 9 shows RR spectra in the 520−640 cm^{-1} region of recombinant sw Mb(III)−NOs. The left part (a) displays the raw spectra of the (A) wild type, (B) Gly64−, (C) Leu64−, (D) Trp29−, (E) Thr68−, and (F) Trp68−Mb, and the right part (b) shows the difference spectra between [Mb(III)−^{14}NO] and [Mb(III)−^{15}NO] for (A) wild type, (B) Gly64, (C) Leu64, (D) Trp29, (E) Thr68, and (F) Trp68 mutants. The band positions and relative intensities in raw spectra are appreciably different among these mutants. In the isotope difference spectra two differential patterns with peak/trough pair are seen around ∼598/588 cm^{-1} and ∼574/562 cm^{-1}. The frequencies for the lower frequency pair are fairly fixed (574∼575 cm^{-1} for ^{14}N^{16}O and 562−564 cm^{-1} for ^{15}N^{16}O), while those for the higher frequency pair are more scattered (593−603 cm^{-1} for ^{14}N^{16}O and 585−591 cm^{-1} for ^{15}N^{16}O). Benko and Yu[31b] assigned the higher and lower frequency pairs to the ν_{Fe-NO} and δ_{FeNO} modes of the Fe(III)−N−O moiety, respectively.

Regarding the ν_{Fe-NO} mode, the Trp29 mutant yields a particularly high frequency, but Trp68 and Thr68 mutants give a low frequency, while the amounts of isotopic frequency shifts of both pairs are alike. This frequency is insensitive to polarity of the 64th residue. Although the FTIR ν_{NO} band is reported at 1927 and 1903 cm^{-1} for native and H64L Mb(III)NO, respectively,[36] no NO-isotope-sensitive Raman band was observed in the 1800−1900 cm^{-1} region for Mb(III)NO in this study. It is noted that the behaviors of Fe−ligand vibrations are quite different between Fe^{II}−CO and Fe^{III}−NO complexes, despite the fact that they have the same number of electrons.

Discussion

The Fe−NO Stretching Mode of Nitrosylmyoglobin. The isotope difference spectrum for ν_{Fe-NO} of MbNO at pH 7.4 (Figure 2a, trace C) is broad, and the shape and position of the NO-associated band are not self-evident in the raw spectra. If the bandwidth was broader than the magnitude of frequency shift, the peak positions in the isotope difference spectra would give a band separation larger than the real frequency shift. To examine this problem, simulations of the isotope difference spectra were carried out by assuming a Gaussian band shape, as applied previously.[37,38] The results for hh native MbNO at neutral pH are illustrated in Figure 10, where traces A, B, C, and D represent the bands assumed for Mb^{14}N^{16}O, Mb^{15}N^{16}O

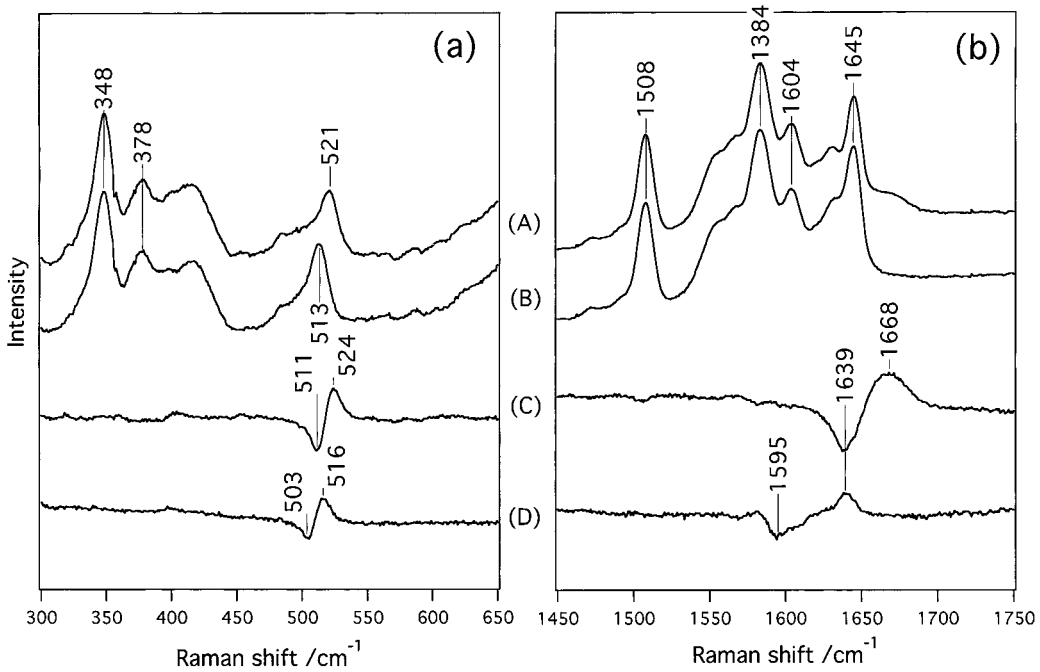

Figure 6. Raman spectra in the 300−650 (a) and 1450−1750 cm^{-1} region (b) of horse heart native MbNO (80 μM) in 50 mM sodium phosphate-acetic acid, pH 4. (A) $Mb^{14}N^{16}O$, (B) $Mb^{15}N^{16}O$, (C) difference spectrum, $Mb^{14}N^{16}O-Mb^{15}N^{16}O$, and (D) difference spectrum $Mb^{15}N^{16}O-Mb^{15}N^{18}O$. For (C) and (D), the ordinate scales are (A) − (B) for (a) and [(A) − (B)] × 2 for (b). Other conditions are the same as those for Figure 2.

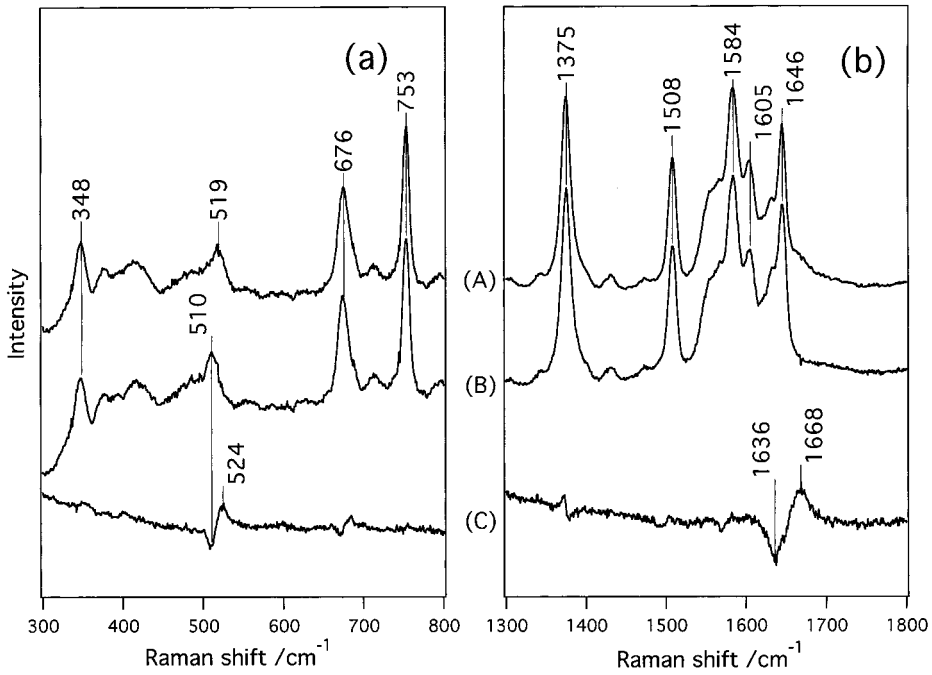

Figure 7. Raman spectra in the 300−650 (a) and 1450−1750 cm^{-1} region (b) of Leu64−MbNO (80 μM) in 50 mM sodium phosphate-acetic acid, pH 4. (A) $Mb^{14}N^{16}O$, (B) $Mb^{15}N^{16}O$, and (C) difference spectrum, $Mb^{14}N^{16}O-Mb^{15}N^{16}O$ {(A) − (B) for (a) and [(A) − (B)] × 2 for (b)}. Other conditions are the same as those for Figure 2.

(left part), and $Mb-{}^{15}N^{18}O$ (right part), experimental difference spectrum, calculated difference spectrum, and residuals in the difference between the experimental and calculated difference spectra, respectively. It was determined from this simulation that the bandwidths were 31 cm^{-1} and the peak position of ν_{Fe-NO} was 552 cm^{-1} for the $^{14}N^{16}O$, 538 cm^{-1} for $^{15}N^{16}O$, and 536 cm^{-1} for $^{15}N^{18}O$ derivatives. Thus, the isotopic frequency shifts between $Fe-{}^{14}N^{16}O$ and $Fe-{}^{15}N^{16}O$ are much smaller (14 cm^{-1}) than the frequency separation between the peak and trough (24 cm^{-1}), and more reasonable. Therefore, it is quite important to determine the band positions by simulation when the bandwidths are larger than the amount of the shift.

Comparison of the Fe−N−O Binding Geometry. The magnitude of isotopic frequency shift depends on binding geometry of a ligand.[39,40] Normal coordinate calculations for a simplified model may provide some suggestions in correlating the observed isotopic frequency shifts with local geometry. In such a simple treatment, a potential function represented by eq 1 was previously applied to MbCO,[38b]

$$2V = K_1(\Delta r_{Fe-NO})^2 + K_2(\Delta r_{N-O})^2 + H(\Delta\theta_{Fe-N-O})^2 + F(\Delta q_{Fe\cdots O})^2 \quad (1)$$

where Δr_{Fe-NO}, Δr_{N-O}, $\Delta\theta_{Fe-N-O}$, and $\Delta q_{Fe\cdots O}$ denote the

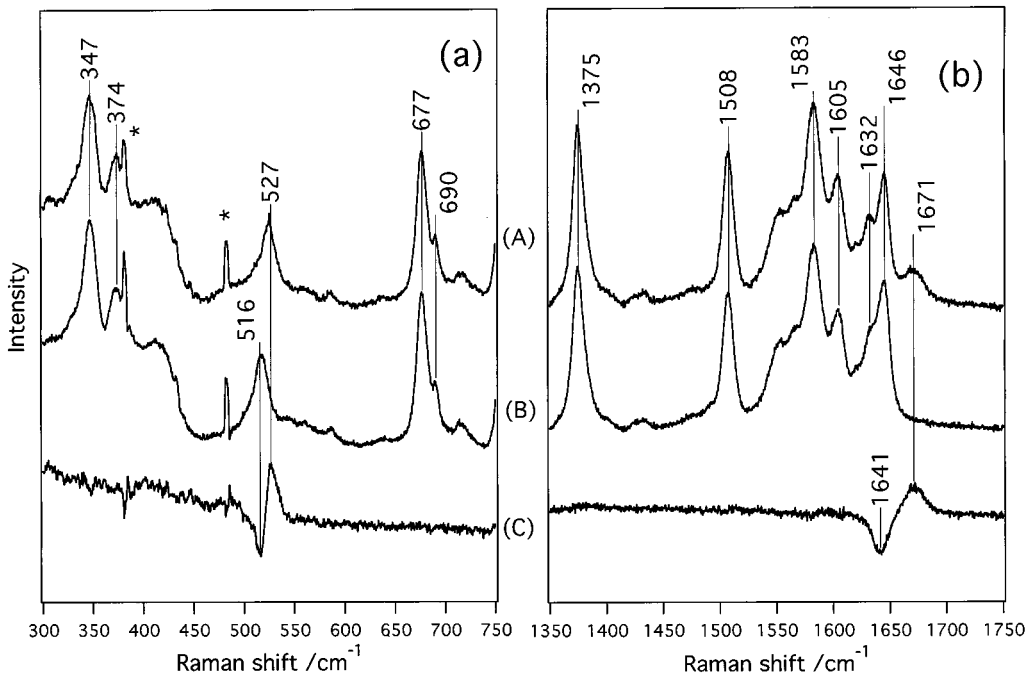

Figure 8. Raman spectra in the 280−740 (a) and 1330−1750 cm^{-1} regions (b) of Fe(II)(PPIX)−NO (80 μM) in 50 mM TEA, pH 7.4, containing 0.5% sodium cholate. (A) Fe(PPIX)^{14}N^{16}O, (B) Fe(PPIX)^{15}N^{16}O, and (C) difference spectrum [= (A) − (B)]. Peaks marked by an asterisk denote the plasma lines from a Kr^+ ion laser. Experimental conditions: excitation, 406.7 nm and 1.5 mW at sample; accumulation time, 50 min.

TABLE 1: Observed Absolute Frequencies and Isotope Shifts of the NO-Associated Raman Bands (cm^{-1} unit)

	ν(Fe−NO)	$\Delta(^{15}N^{16}O)^a$	$\Delta(^{15}N^{18}O)^a$	ν(N−O)	$\Delta(^{15}N^{16}O)^a$	$\Delta(^{15}N^{18}O)^a$
horse native MbNO pH 7	558	26	27	1613	27	68
sperm whale recombinant MbNO pH 7						
wild type	560	29		1613	27	
Gly^{64}	560	23		1631	*b*	
Leu^{64}	560	26		1635	28	69
Trp^{29}	567	24		1608	22	
Thr^{68}	551	25		*b*	*b*	
Trp^{68}	551	25		1615	29	
horse native MbNO pH 4	524	13	16	1668	29	73
sperm whale recombinant MbNO pH 4						
wild type	524	14		1668	32	
Gly^{64}	524	14		1668	32	
Leu^{64}	524	14		1668	32	
Trp^{68}	524	14		1668	32	
Fe(PPIX)NO						
+ sodium cholate	527	11		1671	30	
+BSA	523	12		1668	30	

[a] $\Delta(^{15}N^{16}O)$ and $\Delta(^{15}N^{18}O)$ indicate the isotopic shifts of the $^{15}N^{16}O$ and $^{15}N^{18}O$ adducts from the frequency of the $^{14}N^{16}O$ adduct, respectively. [b] The values of the isotopic shift are not precisely determined due to coupling with porphyrin ring modes.

displacement coordinates for the Fe−NO bond length, N−O bond length, Fe−N−O bond angle, and Fe···O-nonbonding-atoms separation, respectively. The calculated frequencies and isotopic frequency shifts (Δ) from those of $^{14}N^{16}O$ derivatives are compared with the observed ones in Table 2.

For MbNO at neutral pH, the structural parameters except for θ_{Fe-N-O} were transferred from the X-ray crystallographic analysis of six-coordinated ironporphyrin−NO complex,[41] while for MbNO at acidic pH the structural parameters except for θ_{Fe-N-O} were transferred from the X-ray crystallographic analysis of five-coordinated ironporphyrin−NO complex.[41b] The force constants were adjusted by a trial and error method as given in the footnotes of Table 2. In general, $\Delta(^{15}N^{18}O)$ for the Fe−NO stretching mode should be much larger than $\Delta(^{15}N^{16}O)$ for any values of force constants, when the Fe−N−O bond angle (θ_{Fe-N-O}) is larger. However, the observed values for $\Delta(^{15}N^{18}O)$ are not greatly different from those of $\Delta(^{15}N^{16}O)$, suggesting that the Fe−N−O geometry is fairly bent. In contrast, when θ_{Fe-N-O} becomes smaller, the $\Delta(^{15}N^{16}O)$ becomes larger but $\Delta(^{15}N^{18}O)$ becomes smaller for ν_{Fe-NO}.

For the six-coordinated structure, θ_{Fe-N-O} =115° as observed recently for MbNO[42] was used, while other values determined by X-ray structural analysis of Fe^{II}−porphyrin-NOs[41a,b] (θ_{Fe-N-O} = 142° for six-coordinated complex and 149° for five-coordinated complex) and of Hb−NO[43] were not so satisfactory as shown in Table 1 with regard to reproduction of the observed $\Delta(^{15}N^{16}O)$ and $\Delta(^{15}N^{18}O)$. These X-ray values of θ_{Fe-N-O} are larger than the EPR values: 137° for Hb(α)−NO, 130° for Hb(β)−NO;[44] 153° for Mb−NO at 293 K, and 109° for Mb−NO at 77 K.[45] The calculated results for MbNO at pH 4 were obtained with θ_{Fe-N-O} =130°. When θ_{Fe-N-O} =120° or 140° was used, agreements between the calculated and observed $\Delta(^{15}N^{16}O)$ and $\Delta(^{15}N^{18}O)$ were worse than those in Table 2 for any set of force constants.

Comparison of the N−O Stretching with Fe−NO Stretching Modes. Lipscomb et al.[46] reported ν_{Fe-NO} RR bands of

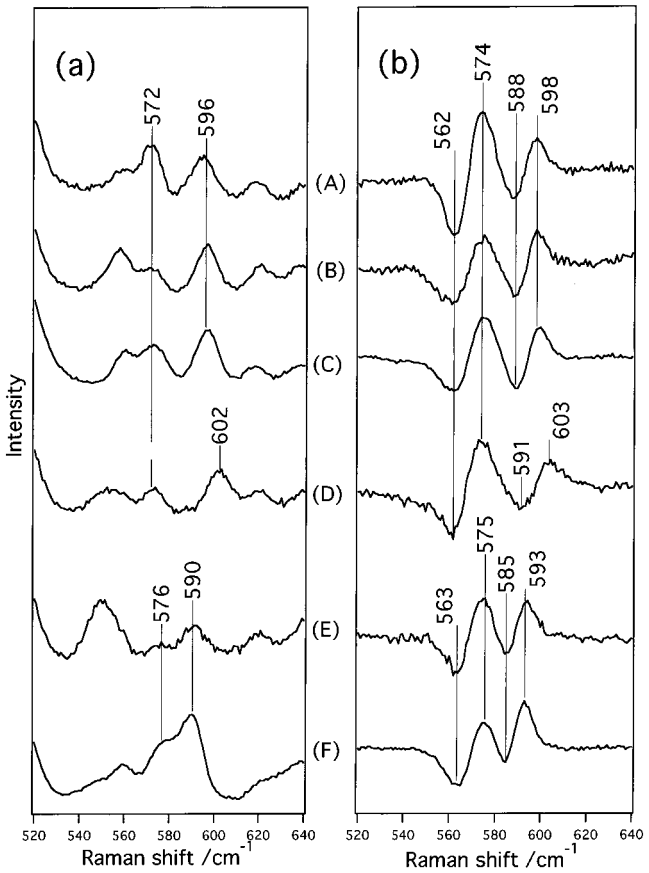

Figure 9. (a) Raman spectra in the 520−640 cm^{-1} region of recombinant Mb(III)-NO in 50 mM sodium phosphate, pH 7.4. (A) Wild-type $Mb^{14}N^{16}O$, (B) Gly64−$Mb^{14}N^{16}O$, (C) Leu64−$Mb^{14}N^{16}O$, (D) Trp29−$Mb^{14}N^{16}O$, (E) Thr68−$Mb^{14}N^{16}O$, and (F) Trp68−$Mb^{14}N^{16}O$. (b) The difference spectra between [$Mb(III)^{14}N^{16}O$] and [$Mb(III)^{15}N^{16}O$]. (A) Wild type, (B) Gly64, (C) Leu64, (D) Trp29, (E) Thr68, and (F) Trp68. Experimental conditions: concentration, 50 μM; excitation, 422.6 nm and 6 mW at sample; accumulation time, 5 min.

several six-coordinated (OEP)Fe^{II}(L)−NO complexes at 524−527 cm^{-1}. Unexpectedly, these frequencies are closer to ν_{Fe-NO} values of the five- than six-coordinate heme-NO adducts observed in this work. We tried to detect Raman bands of *N*-methylimidazole (N-MeIm) complex of Fe^{II}protoporphyrin [(N−MeIm) Fe^{II}(PPIX)−NO] as a relevant model compound of NO-bound heme proteins, but it was unsuccessful. This was because of the fact that the Fe−(N−MeIm) bond was broken when NO was bound to its trans position.

Wayland and Olson[47] reported that $Fe^{II}(OEP)(NO)_2$ could be readily formed in the absence of any base to become a trans ligand. In the case of Fe^{II}(PPIX), however, the bis(nitrosyl) compound has never been identified so far. This may suggest that the Fe−NO bond of (N−MeIm)−Fe^{II}(OEP)−NO is different from that of (N−MeIm)−Fe^{II}(PPIX)−NO and also that the trans effects of NO are affected by the side chains of porphyrin ring. It must be the protein effect that the Fe−His bond is retaining in MbNO at neutral pH despite the same macrocycle as protoporphyrin IX.

There are a few reports about the ν_{Fe-NO}, δ_{FeNO}, and ν_{NO} Raman bands of six-coordinated heme−NO adducts. The ν_{Fe-NO} frequencies of MbNO (556 cm^{-1}),[31b] HbNO (556 cm^{-1}),[33b,34] and FixL−NO (558 cm^{-1}),[19b] which have commonly His residue at the trans position of NO, are alike, but are distinctly higher than those of cystein-coordinated heme proteins such as $P450_{cam}$ (547∼553 cm^{-1}),[33a] chloroperoxidase (CPO) (542 cm^{-1}),[48] and nitric oxide synthase (NOS) (536∼542 cm^{-1}).[49] The coordination of S^- at the trans position of NO seems to weaken the Fe^{II}−NO bond but the absence of the trans ligand much weakens the Fe^{II}−NO bond as judged from the ν_{Fe-NO} frequencies.

Recombinant WT MbNO gave practically the same ν_{Fe-NO} frequency as that of the hh native MbNO at neutral pH. Although the Fe−$^{15}N^{16}O$ stretching bands of Gly64− and Leu64−MbNO appear slightly different from those of WT MbNO [Figure 3a, traces A−C], it is probably caused by overlapping of a broad porphyrin band around 530−540 cm^{-1} (Figure 3a) or a vibrational coupling with a porphyrin vibration. Therefore, we conclude that the substitution of the distal His with an aliphatic amino acid residue yields little effects on the ν_{Fe-NO} frequency.

On the other hand, Trp29−MbNO gave the ν_{Fe-NO} band at a higher frequency (567 cm^{-1}), while Trp68− and Thr68−MbNO gave it at a lower frequency (551 cm^{-1}) than that of WT MbNO (Figure 3). Hu and Kincaid[33a] discussed the dependence of the ν_{Fe-NO} and δ_{FeNO} frequencies on the geometry of the Fe−N−O moiety on the basis of normal coordinate calculations. According to their results, the Fe−N−O bond angle influences both ν_{Fe-NO} and δ_{FeNO}, whereas tilting of the Fe−N bond from the normal of heme plane influences only ν_{Fe-NO} frequency. Since the observed $\Delta(^{15}N^{16}O)$ values of these three mutants are alike and also the same as the $\Delta(^{15}N^{16}O)$ value of the WT MbNO, the Fe−N−O bond angle would be unaltered by this mutation. Instead, appreciable tilting of the Fe−N bond might be present in common and might change the ν_{Fe-NO} frequencies among these mutants. Hori et al.[45] also suggested from EPR spectra that NO of MbNO was tilting due to steric hindrance. It is inferred that tilting of NO group is decreased in Trp29−MbNO and increased in Trp68− and Thr68−MbNO due to changes of the steric effects in the heme pocket. We point out that the perturbation effects on the bound ligand by nearby residues in MbNO are close to those in the MbO_2 mutants[50] but distinct from the perturbation effect of MbCO.[28,51]

Mb(III)−NO complexes show the same tendencies in the steric effects as those for Mb(II)−NO. The RR bands assigned to ν_{Fe-NO} and δ_{FeNO} are observed at 596 and 572 cm^{-1} in the raw spectrum, respectively, for WT Mb(III)−NO (Figure 9a, trace A). The ν_{Fe-NO} frequency remains unaltered by the substitution of the distal His, while the ν_{NO} frequency is distinctly different between the WT and H64L Mbs.[36] The ν_{Fe-NO} band is shifted by 5 cm^{-1} toward higher and lower frequencies upon the substitution of 68th and 29th residue, respectively. This is confirmed by the isotope difference spectra shown in Figure 9b. In contrast with the ν_{Fe-NO} bands, the δ_{FeNO} frequencies are scarcely shifted among these mutants. The amount of frequency shifts is at most 2 cm^{-1} as seen for the 68th mutant. Generally, a frequency of δ_{FeNO} is more sensitive to the Fe−N−O bond angle than that of ν_{Fe-NO}. Therefore, the changes of ν_{Fe-NO} frequencies of Mb(III)−NO by the mutation are considered to be caused by changes in the tilting angle of the Fe−N bond but not by changes in the Fe−N−O bond angle. This may be one of the reasons for the differences between CO and NO in the behavior of the Fe-ligand stretching frequencies.

NO of MbNO is stabilized by hydrogen bonding from distal His.[52] The ν_{NO} frequency should be sensitive to the hydrogen bonding from the protein moiety to NO. The ν_{NO} Raman band of WT MbNO was observed at 1613 cm^{-1}, which is close to the ν_{NO} frequencies of a model compound in aprotic solvents [1616−1618 cm^{-1} for (N−MeIm)−Fe^{II}(PPIX)−NO)].[53,54] In contrast with ν_{Fe-NO}, the effects of mutation were clearly seen in the ν_{NO} frequency. In fact, distal His mutants (Gly64− and Leu64−MbNO) gave ν_{NO} at frequencies higher by 18−22 cm^{-1}

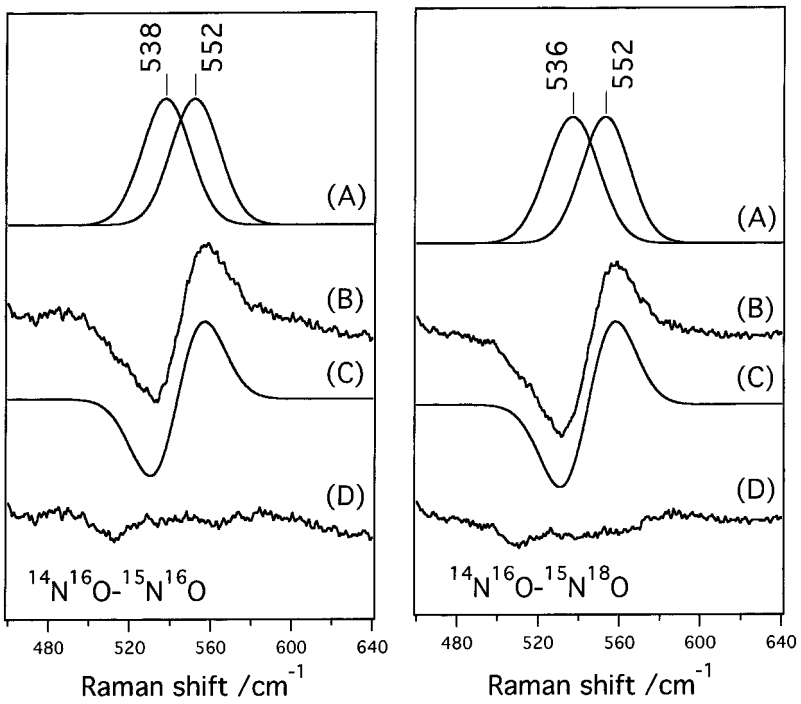

Figure 10. Simulation of the difference spectra for the Fe−NO stretching mode of Mb(II)-NO at pH 7.4. (A) Assumed bands (Gaussian band shape), (B) observed difference spectra, (C) calculated difference spectra, (D) residuals in the difference between the observed and calculated difference spectra [= (B) − (C)]. The left and right panels show the results for the isotope combinations of $^{14}N^{16}O-^{15}N^{16}O$ and $^{14}N^{16}O-^{15}N^{18}O$, respectively.

TABLE 2: Calculated Frequencies of the Isolated Fe−N−O Unit and Observed Frequencies of MbNO and Fe(PPIX)NO[a]

		$^{14}N^{16}O$		$^{15}N^{16}O(\Delta^d)$		$^{15}N^{18}O(\Delta^d)$	
		obs	calcd	obs	calcd	obs	calcd
Mb−NO, pH 7.4[b]	ν(N−O)	1613	1612	27	29	68	72
	ν(Fe−NO)	552	552	14	14	16	16
	δ(Fe−N−O)	∼454	451	*e*	4	*e*	18
Mb−NO, pH 4[c]	ν(N−O)	1668	1668	29	30	73	74
	ν(Fe−NO)	524	524	13	12	16	15
	δ(Fe−N−O)	∼402	402	*e*	6	*e*	16

[a] ln cm^{-1} unit. [b] Parameters used for calculations are the following: r(Fe−N) = 1.74 Å, r(N−O) = 1.12 Å, K_1(Fe−N) = 1.76 mdyn/Å, K_2(N−O) = 11.00 mydn/Å, H(Fe−N−O) = 0.57 mdyn Å, F(Fe···O) = 1.20 mdyn/Å, θ(Fe−N−O) = 1.15°. [c] Parameters used for calculations are the following: r(Fe−N) = 1.72 Å, r(N−O) = 1.12 Å, K_1(Fe−N) = 1.70 mdyn/Å, K_2(N−O) = 11.84 mydn/Å, H(Fe−N−O) = 0.39 mdyn Å, F(Fe···O) = 1.08 mdyn/Å, θ(Fe−N−O) = 130°. [d] The values indicate isotope shift. [e] Not determined.

than those of WT, but other mutants did not alter the ν_{NO} frequency greatly. Removal of hydrogen bond in Gly64 and Leu64 mutants might restore an N═O double-bond character from the more polarized $N^{\delta+}-O^{\delta-}$ bond of the His64 mutants, causing a high-frequency shift of ν_{NO}. Since the heme pocket of Mb is surrounded by hydrophobic amino acid residues, the heme-bound NO without any hydrogen bonding corresponds to an NO model compound in apolar solvents.

Comparison of MbNO with MbCO suggests that the ν_{Fe-CO} frequency is more sensitive to the distal environments than the ν_{Fe-NO} frequency. There are inverse linear relationships between ν_{CO} and ν_{Fe-CO} frequencies owing to the back-bonding from Fe to CO.[38c,39,40,55−57] Accordingly, the ν_{CO} and ν_{Fe-CO} frequencies of Mb mutants change simultaneously upon replacement of His64: 1945 and 510 cm^{-1} for WT−MbCO, 1965 and 505 cm^{-1} for Gly64−MbCO, and 1965 and 490 cm^{-1} for Leu64−MbCO, respectively.[28,51a] This is distinct from the NO and O_2 adducts of hemes, for which other factors than the back-donation, presumably steric hindrance, may play an important role and as a result, the ν_{NO} and ν_{Fe-NO} frequencies seem to have no correlation.

For five-coordinated heme−NO-adducts of heme proteins at neutral pH, RR spectra have been reported for FixL−NO,[19b] the α subunit of T-state HbA-NO[16b] and sGC−NO.[7,17] Raman bands of MbNO at pH 4 are much weaker in intensity than those of six-coordinated species, and only major bands are observable even with 406.7 nm excitation. The Raman spectrum of acidic MbNO was identical with that of Fe^{II}(PPIX)-NO in 0.5% BSA solution (data not shown), but definitely different from the spectrum of sGC−NO.[7] The ν_{Fe-NO} frequency of Fe^{II}(PPIX)-NO in sodium cholate (527 cm^{-1}) is slightly higher than those of other five-coordinated heme−NOs (524 cm^{-1}). The higher ν_{Fe-NO} frequency of Fe^{II}(PPIX)-NO in sodium cholate is presumably caused by the micelle formation, which may remove the hydrogen bonding to NO.

Maxwell and Caughey[53] reported that the ν_{NO} frequency of the five-coordinate Fe^{II}−(PPIX dimethyl ester)−NO complex becomes higher in more apolar organic solvents (1669 cm^{-1} in $ClCH_2CH_2Cl$, 1676 cm^{-1} in $CHCl_3$, and 1684 cm^{-1} in CCl_4). Yoshimura[58] demonstrated the presence of a linear correlation between ν_{NO} frequencies and solvent polarities. Nevertheless, the five-coordinated NO−heme in Mb at low pH seems to receive no perturbation from the surrounding amino acid residues, because the ν_{NO} frequencies of Mb−NO at pH 4 and Fe^{II}(PPIX)−NO were alike, and furthermore, the point mutation of the distal His did not change ν_{NO} frequencies. Presumably the heme is not settled at a fixed position in the heme pocket owing to cleavage of the Fe−His bond, which ordinarily fixes the heme in place. In addition, at pH 4 the distal histidine is protonated and swings out into the solvent preventing hydrogen bond formation with the bound ligand.[24]

Acknowledgment. This study was supported by Grant-in-Aids for Scientific Research for Priority Areas (Molecular

Biometallics, Grant 08249106) from the Ministry of Education, Science, Sports, and Culture, Japan, and by grants from the U.S. National Institutes of Health, Grants GM35649 and HL47020, The Robert A. Welch Foundation Grant C-612, and the W. M. Keck Center for Computational Biology.

References and Notes

(1) McMillan, K.; Bredt, D. S.; Hirsch, D. J.; Snyder, S. H.; Clark, J. E.; Masters, B. S. S. *Proc. Natl. Acad. Sci. U.S.A.* **1992**, *89*, 11141−11145.
(2) White, L A.; Marletta, M. A. *Biochemistry* **1992**, *31*, 6627−6631.
(3) Stuehr, D. J.; Ikeda-Saito, M. *J. Biol. Chem*. **1992**, *267*, 20547−20550.
(4) Gerzer, R.; Bohme, E.; Hofmann, F.; Shultz, G. *FEBS Lett*. **1981**, *132*, 71−74.
(5) Abu-Soud, H. M.; Wang, J.; Rousseau, D. L.; Fukoto, J. M.; Ignarro, L. J.; Stuehr, D. J. *J. Biol. Chem*. **1995**, *270*, 22997−23006.
(6) Ignarro, L. J.; Degnan, J. N.; Baricos, W. H.; Kadowitz, P. J.; Wolin, M. S. *Biochim. Biophys. Acta* **1982**, *718*, 49−59.
(7) Tomita, T.; Ogura, T.; Tsuyama, S.; Imai, Y.; Kitagawa, T. *Biochemistry* **1997**, *36*, 10155−10160.
(8) Springer, B. A.; Sligar, S. G.; Olson, J. S.; Phillips, G. N., Jr. *Chem. Rev*. **1994**, *94*, 699−714.
(9) Olson, J. S.; Phillips, G. N., Jr. *J. Biol. Chem*. **1996**, *271*, 17593−17596.
(10) Giardina, B.; Amiconi, G. *Methods Enzymol.* **1981**, *76*, 417−427.
(11) Moore, E. G.; Gibson, Q. H. *J. Biol. Chem.* **1976**, *251*, 2788−2784.
(12) Hoshino, M.; Maeda, M.; Konishi, R.; Seki, H.; Ford, P. C. *J. Am. Chem. Soc.* **1996**, *118*, 5702−5707.
(13) Perutz, M. F. *Nature (London)* **1970**, *228*, 726−734.
(14) (a) Nagai, K.; Kitagawa, T.; Morimoto, H. *J. Mol. Biol.* **1980**, *136*, 271−289. (b) Nagai, K.; Kitagawa, T. *Proc. Natl. Acad. Sci. U.S.A.* **1980**, *77*, 2033−2037.
(15) Perutz, M. F.; Kilmartin, J. V.; Nagai, K.; Szabo, A.; Simon, S. R. *Biochemistry* **1976**, *15*, 378−387.
(16) (a) Nagai, K.; Yoshida, S.; Sakamoto, H.; Hori, H. *Biochim. Biophys. Acta* **1978**, *532*, 17−28. (b) Nagai, K.; Welborn, C.; Dolphin, D.; Kitagawa T. *Biochemistry* **1980**, *19*, 4755−4761.
(17) Deinum, G.; Stone, J. R.; Babcock, G. T.; Marletta, M. A. *Biochemistry* **1996**, *35*, 1540−1547.
(18) (a) Stone, J. R.; Marletta, M. A. *Biochemistry* **1994**, *33*, 5636−5640. (b) Stone, J. R.; Marletta, M. A. *Biochemistry* **1996**, *35*, 1093−1099.
(19) (a) Rodgers, K. R.; Lukat-Rodgers, G. S.; Barron, J. A. *Biochemistry* **1996**, *35*, 9539−9548. (b) Lukat-Rodgers, G. S.; Rodgers, K. R. *Biochemistry* **1997**, *36*, 4178−4187.
(20) Winkler, W. C.; Gonzalez, G.; Wittenberg, J. B.; Hille, R.; Dakappagari, N.; Jacob, A.; Gonzalez, L. A.; Gilles-Gonzalez, M. A. *Chem. Biol*. **1996**, 841−850.
(21) (a) Kitagawa, T.; Nagai, K.; Tsubaki, M. *FEBS Lett*. **1979**, *104*, 376−378. (b) Teraoka, J.; Kitagawa, T. *J. Biol. Chem.* **1981**, *256*, 3969−3977.
(22) Duprat, A. F.; Traylor, T. G.; Wu, G.-Z.; Coletta, M.; Sharma, V. S.; Walda, K. N.; Magde, D. *Biochemistry* **1995**, *34*, 2634−2644.
(23) Ascenzi, P.; Brunori, M.; Coletta, M.; Desideri, A. *Biochem. J*. **1989**, *258*, 473−478.
(24) Yang, F.; Phillips, G. N., Jr. *J. Mol. Biol*. **1996**, *256*, 762−774.
(25) Sage, J. T.; Morikis, D.; Champion, P. M. *Biochemistry* **1991**, *30*, 1227−1237.
(26) Ramsden, J.; Spiro, T. G. *Biochemistry* **1989**, *28*, 3125−3128.
(27) (a) Mukai, M.; Nagano, S.; Tanaka, M.; Ishimori, K.; Morishima, I.; Ogura, T.; Watanabe, Y.; Kitagawa, T. *J. Am. Chem. Soc*. **1997**, *119*, 1758−1766. (b) Tanaka, M.; Ishimori, K.; Mukai, M.; Kitagawa, T.; Morishima, I. *Biochemistry* **1997**, *36*, 9889−9898.
(28) Li, T.; Quillin, M. L.; Phillips, G. N., Jr.; Olson, J. S. *Biochemistry* **1994**, *33*, 1433−1446.
(29) (a) Springer, B. A.; Egeberg, K. D.; Sliger, S. G.; Rohlfs, R. J.; Mathews, A. J.; Olson, J. S. *J. Biol. Chem.* **1989**, *264*, 3057−3060. (b) Egeberg, K. D.; Springer, B. A.; Martinis, S. G.; Sliger, S. G.; Morkis, D.; Champion, P. M. *Biochemistry* **1990**, *29*, 9783−9791. (c) Egeberg, K. D.; Springer, B. A.; Sliger, S. G.; Carver, T. E.; Rohlfs, R. J.; Olson, J. S. *J. Biol. Chem.* **1990**, *265*, 11788−11795. (d) Carver, T. E.; Brantley, R. E.; Singleton, E. W.; Arduini, R. M.; Quillin, M. L.; Phillips, G. N., Jr.; Olson, J. S. *J. Biol. Chem.* **1992**, *265*, 14443−14450.
(30) Decatur, S. M.; Franzen, S.; DePhillis, G. D.; Dyer, R. B.; Woodruff, W. H.; Boxer, S. G. *Biochemistry* **1996**, *35*, 4939−4944.
(31) (a) Tsubaki, M.; Yu, N.-T. *Biochemistry* **1982**, *21*, 1140−1144. (b) Benko, B.; Yu, N.-T. *Proc. Natl. Acad. Sci*. **1983**, *80*, 7042−7046.
(32) Zhao, X.-J.; Sampath, V.; Caughey, W. S. *Biochem. Biophys. Res. Commun.* **1994**, *204*, 537−543.
(33) (a) Hu, S.; Kincaid, J. R. *J. Am. Chem. Soc.* **1991**, *113*, 2843−2850. (b) Hu, S.; Kincaid, J. R. *J. Am. Chem. Soc.* **1991**, *113*, 9760−9766.
(34) Chottard, J. C.; Mansuy, D. *Biochem. Biophys. Res. Commun*. **1977**, *77*, 1333−1338.
(35) Schelvis, J. P. M.; Zhao, Y.; Marletta, M. A.; Babcock, G. T. *Biochemistry* **1998**, *37*, 16289−16297.
(36) Miller, L. M.; Pedraza, A. J.; Chance, M. R. *Biochemistry* **1997**, *36*, 12199−12207.
(37) Hu, S.; Smith, K. M.; Spiro, T. G. *J. Am. Chem. Soc*. **1996**, *118*, 12638−12646.
(38) (a) Hirota, S.; Ogura, T.; Appelman, E. H.; Shinzawa-Itoh, K.; Yoshikawa, S.; Kitagawa, T. *J. Am. Chem. Soc.* **1994**, *116*, 10564−10570. (b) Hirota, S.; Ogura, T.; Shinzawa-Itoh, K.; Yoshikawa, S.; Kitagawa, T. *J. Phys. Chem.* **1996**, *100*, 15274−15279. (c) Hirota, S.; Ogura, T.; Shinzawa-Itoh, K.; Yoshikawa, S.; Nagai, M.; Kitagawa, T. *J. Phys. Chem.* **1994**, *98*, 6652−6660.
(39) Li, X.-Y.; Czernuszewicz, R. S.; Kincaid, J. R.; Spiro, T. G. *J. Am. Chem. Soc.* **1989**, *111*, 7012−7023.
(40) Nagai, M.; Yoneyama, Y.; Kitagawa, T. *Biochemistry* **1991**, *30*, 6495−6503.
(41) (a) Scheidt, W. R.; Frisse, M. E. *J. Am. Chem. Soc*. **1975**, *97*, 17−21. (b) Scheidt, W. R.; Piciulo, P. L. *J. Am. Chem. Soc.* **1976**, *98*, 1913−1919.
(42) Brucker, E. A.; Olson, J. S.; Ikeda-Saito, M.; Phillips, G. N., Jr. *Proteins: Struct., Funct., Genet.* **1998**, in press.
(43) Deatherage, J. F.; Moffat, K. *J. Mol Biol.* **1979**, *134*, 401−417.
(44) Utterback, S. G.; Doetschman, D. C.; Szumowski, J.; Rigos, A. K. *J. Chem. Phys.* **1983**, *78*, 5874−5880.
(45) Hori, H.; Ikeda-Saito, M.; Yonetani, T. *J. Biol. Chem.* **1981**, *256*, 7849−7855.
(46) Lipscomb, L. A.; Lee, B.-S.; Yu, N.-T. *Inorg. Chem.* **1993**, *32*, 281−286.
(47) Wayland, B. B.; Olson, L. W. *J. Am. Chem. Soc*. **1974**, *96*, 6037−6041.
(48) Hu, S.; Kincaid, J. R. *J. Biol. Chem.* **1993**, *268*, 6189−6193.
(49) Wang, J.; Rousseau, D. L.; Abu-Soud, H. M.; Stuehr, D. J. *Proc. Natl. Acad. Sci. U.S.A.* **1994**, *91*, 10512−10516.
(50) Hirota, S.; Li, T.; Phillips, G. N., Jr.; Olson, J. S.; Mukai, M.; Kitagawa, T. *J. Am. Chem. Soc*. **1996**, *33*, 7845−7846.
(51) (a) Sakan, Y.; Ogura, T.; Kitagawa, T.; Fraunfelter, F. A.; Mattera, R.; Ikeda-Saito, M. *Biochemistry* **1993**, *32*, 5815−5824. (b) Nakashima, S.; Kitagawa, T.; Olson, J. S. *Chem. Phys*. **1998**, *229*, 323−336.
(52) (a) Eich, R. Ph.D. Dissertation, Rice University, 1997. (b) Oson, J. S.; Phillips, G. N., Jr. *J. Bio. Inorg. Chem*. **1997**, *2*, 544−552.
(53) Maxwell, J. C.; Caughey, W. S. *Biochemistry* **1976**, *15*, 388−396.
(54) Yoshimura, T. *Bull. Chem. Soc. Jpn*. **1978**, *51*, 1237−1238.
(55) (a) Tsubaki, M.; Srivastava, R. B.; Yu, N. T. *Biochemistry*, **1982**, *21*, 1132−1140. (b) Yu, N. T.; Kerr, E. A. In *Biological Application of Raman Spectroscopy*; Spiro, T. G., Ed.; Wiley-Interscience: New York, 1988; Vol. 3, pp 40−95.
(56) Park, K. D.; Guo, K.; Adebodun, F.; Chiu, M. L.; Sliger, S. G.; Oldfield, E. *Biochemistry* **1991**, *30*, 2333−2347.
(57) Ray, G. B.; Li, X.-Y.; Ilbers, J. A.; Sessler, J. L.; Spiro, T. G. *J. Am. Chem. Soc.* **1994**, *116*, 162−176.
(58) Yoshimura, T. *Arch. Biochem. Biophys*. **1983**, *220*, 167−178.